

Optimization of fluorinated orthoformate based electrolytes for practical high-voltage lithium metal batteries

Xia Cao^a, Lianfeng Zou^b, Bethany E. Matthews^a, Linchao Zhang^{a,1}, Xinzi He^{a,c}, Xiaodi Ren^a, Mark H. Engelhard^b, Sarah D. Burton^b, Patrick Z. El-Khoury^d, Hyung-Seok Lim^a, Chaojiang Niu^a, Hongkyung Lee^a, Chunsheng Wang^c, Bruce W. Arey^a, Chongmin Wang^b, Jie Xiao^a, Jun Liu^a, Wu Xu^{a,*}, Ji-Guang Zhang^{a,2,*}

^a Energy and Environment Directorate, Pacific Northwest National Laboratory, Richland, WA 99354, United States

^b Environmental Molecular Sciences Laboratory, Pacific Northwest National Laboratory, Richland, Washington 99354, United States

^c Department of Chemical and Biomolecular Engineering, University of Maryland, College Park, MD 20742, USA

^d Physical Sciences Division, Pacific Northwest National Laboratory, Richland, Washington 99354, United States

ARTICLE INFO

Keywords:

Electrolyte
Tris(2,2,2-trifluoroethyl) orthoformate
Localized high-concentration electrolyte
Lithium anode
Lithium metal battery
High voltage

1. Introduction

Increasing demand for high energy density batteries for portable electronic devices, electric vehicles, and large-scale grid energy storage, has revitalized interest in lithium (Li) metal batteries (LMBs) in recent years [1–10]. To maximize battery operation voltages, as well as specific energy densities, high-voltage, nickel-rich, layered cathodes, such as $\text{LiNi}_{0.8}\text{Mn}_{0.1}\text{Co}_{0.1}\text{O}_2$ (NMC811), are often paired with a Li metal anode (LMA) to form high voltage LMBs [11,12]. However, significant challenges still exist hindering the use of LMBs in practice [12]. On the anode side, highly porous and dendritic/mossy Li deposition often occurs in LMBs due to excessive and uncontrollable side reactions between the Li metal and electrolyte. These side reactions not only lead to low Coulombic efficiency (CE), poor Li utilization and limited cycle life, but also lead to great safety concerns because of the severe volumetric expansion and potential dendrite penetration through the separator [6,7,13–15]. On the cathode side, the oxidative decomposition of the electrolyte at high voltages remains one of the biggest obstacles because it increases the cell resistance and accelerates electrolyte consumption and gas generation [16–18]. Since the liquid electrolyte is in direct contacts with both LMA and cathode in the battery, the electrolyte is in in-

timite contact with both the LMA and the cathode, therefore the chemical nature of the electrolyte often determines the electrode/electrolyte interphases and thus dictates the battery performance [19]. In this context, there is an urgent need to develop advanced electrolytes that are suitable and safe for high voltage LMBs [20–22].

The ideal electrolyte needs to be stable against both the Li anode and the high voltage cathode [23,24]. However, all known electrolyte solvents are thermodynamically unstable against strongly reducing Li metal at low voltages and oxidizing cathodes at high voltages [7,25]. In practice, the stability of electrolytes towards both the anode and the cathode relies on the formation of stable electrode/electrolyte interphases. The interphases are generated during the initial electrolyte-electrode interactions, and suppress subsequent interactions between the electrodes and the electrolyte [26]. However, perfect electrode/electrolyte interphases, including solid electrolyte interphase (SEI) on the anode and a cathode electrolyte interphase (CEI) on the cathode, are rarely seen in batteries, because both the SEI and the CEI need to be homogenous and stable during cycling [13,26]. This is especially challenging if the electrode materials, such as LMA or a silicon anode, experience large volume changes during charge/discharge processes, which lead to continuous break down and reformation of new

* Corresponding authors.

E-mail addresses: wu.xu@pnnl.gov (W. Xu), jiguang.zhang@pnnl.gov (J.-G. Zhang).

¹ Current address: Key Laboratory of Materials Physics, Institute of Solid State Physics, Chinese Academy of Sciences, Hefei, Anhui 230026, China

² Lead contact

interphase layers [27–29]. The breakdown and reformation of the interphase layers will not only corrode the electrode, and consume electrolytes, but they often lead to the growth of high impedance interphase layers that ultimately result in early battery failure.

Over the last few years, a significant breakthrough in electrolyte development has been made by increasing the salt concentration in selected salt–solvent combinations, forming so called high concentration electrolytes (HCEs) or super concentrated electrolytes (SCEs), which dramatically reduce the number of free solvent molecules in the electrolyte while increasing the number of contact ion pairs (CIPs) and aggregates (AGGs) [30–32]. As a result, salt anions are reduced prior to solvent molecule reduction and form an anion-derived SEI due to the anions' reduced lowest unoccupied molecular orbital (LUMO) energy by extensively coordinating to Li^+ . This anion-derived SEI features better ionic conductivity and mechanical strength when compared to the solvent-derived SEI. However, HCEs or SCEs also exhibit several disadvantages such as high viscosity, low conductivity, poor wettability between electrode and separator, and high cost, which ultimately limit their practical applications [30]. One solution is to use “inert” solvents (also called diluents) to dilute the HCEs and form localized high-concentration electrolytes (LHCEs), which effectively decreases the viscosity and salt concentration of the electrolyte while maintaining high coordination clusters in the electrolyte [30,33–35]. The reported “inert” solvents normally belong to fluorinated ethers, such as bis(2,2,2-trifluoroethyl) ether, 1,1,2,2-tetrafluoroethyl-2,2,3,3-tetrafluoropropyl ether, and 1H,1H,5H-octafluoropentyl-1,1,2,2-tetrafluoroethyl ether [23,30,33–35]. In a recent study, Cao et al. reported a new solvent, tris(2,2,2-trifluoroethyl) orthoformate (TFEO), as a promising electrolyte component for LMBs [24,36]. It has high oxidative stability, a high boiling point and low viscosity [24]. The TFEO based electrolyte, 1 M lithium bis(fluorosulfonyl)imide (LiFSI) in 1,2-dimethoxyethane (DME) and TFEO (1:9 by wt. or 1.2:3 by mol.), shows significantly improved electrochemical performance compared to conventional carbonate- and ether- based electrolytes by generating both a monolithic SEI layer on the LMA and a LiF-enriched CEI layer on the Ni-rich NMC cathode. However, the exact role of the TFEO in the electrolyte is still not well understood based on that previous work.

In this study we investigated the solvation structures of TFEO based electrolytes with different compositions. It was found that TFEO enables the formation of localized high-concentration cation/anion aggregation clusters and accelerates the anion decomposition on the Li metal surface to form a salt derived SEI. By fine tuning the electrolyte compositions, TFEO based electrolytes were tailored to obtain the best results for LMBs under different testing conditions. With an optimized electrolyte, an LMB with NMC811 cathode can retain more than 80% capacity in 200 stable cycles under very challenging conditions with 4.2 mAh cm^{-2} NMC811, 50 μm Li and 3 g (Ah) $^{-1}$ electrolyte. The fundamental understanding on the optimization of the electrolytes based on different testing conditions can guide the rational design of new electrolytes for the next generation LMBs.

2. Experimental procedures

2.1. Electrolyte and electrode preparation

The electrolytes were prepared by dissolving LiFSI in DME or DME/TFEO mixtures inside an MBraun glovebox filled with purified argon, where the moisture and oxygen content was less than 1 ppm. LiFSI was received from Nippon Shokubai Co. Ltd (Tokyo, Japan), and used after drying at 120 °C for 24 h. Battery grade DME was used as received from Goton, Inc. (Fremont, CA, USA). TFEO was purchased from SynQuest Laboratories (Alachua, FL, USA) and dried with pre-activated 4 $\bar{\text{A}}$ molecular sieves before use. The NMC811 cathodes were prepared by slurry coating on Al foil. The cathode consisted of 96 wt.% NMC811, 2 wt.% Super C65 as conductive carbon, and 2 wt.% PVDF as binder

[36]. Two different areal capacity loadings were used, one coating was about 1.5 mAh cm^{-2} , and the other was about 4.2 mAh cm^{-2} . The cathode was punched into 1.27 cm^2 disks and dried at 120 °C overnight before use.

2.2. Electrochemical tests

CR2032 coin cells kits from MTI Corporation were used for cell testing. The Li CE was measured in Li||Cu cells using the standard CE protocol (method 3 with Q_T of 5 mAh cm^{-2} , Q_C of 1 mAh cm^{-2} and n of 10) reported in a previous work [37]. Li deposition morphologies were measured by depositing 1 mAh cm^{-2} Li on Cu substrate at a current of 0.5 mA cm^{-2} .

For Li||Cu cells, a piece of Cu foil cathode, a piece of polyethylene (PE) separator (Asahi Hi-Pore, Japan), and a Li chip (250 μm thick, 1.50 cm diameter, from MTI) were sandwiched together and crimped inside the argon-filled glovebox after filling 75 μL electrolyte. The Li||Li cells were also assembled in the same way by replacing the Cu foil in Li||Cu cells with a Li chip. Li||Li cells were evaluated by plating/stripping 1 mAh cm^{-2} of Li at a current density of 0.5 mA cm^{-2} . The Li||NMC811 cells were assembled using the Al-clad positive cans and an extra Al foil with 1.90 cm diameter was placed in between the cathode disk and the Al-clad positive can.

The Li||NMC811 cells tested under the moderate condition had a NMC811 (1.5 mAh cm^{-2}) disk for the cathode, with 50 \pm 2 μm thick Li on Cu foil (China Energy Lithium Co., Ltd., Tianjin, China) for the anode and 75 μL of electrolyte in each cell. The Li||NMC811 cells were tested between 2.8 and 4.4 V at C/3 charge and discharge, with a CV step at 4.4 V till the current to C/20 or time of 1 h after two formation cycles at C/10, where 1C was \sim 1.5 mA cm^{-2} (200 mA g^{-1}).

For the Li||NMC811 cells under the practical condition, a 4.2 mAh cm^{-2} NMC811 disk was used for the cathode and only 15 μL electrolyte was sealed in the cell. The cells were tested in the same voltage range at C/10 charge and C/3 discharge after two formation cycles at C/10 charge/discharge, where 1C was \sim 4.2 mA cm^{-2} (200 mA g^{-1}). The impedance was measured at open circuit voltage (OCV) at 0% state of charge (SOC) after every 20 cycles to monitor resistance changes in the Li||NMC811 cells during cycling. AC impedance spectra were recorded in potentiostatic mode on a CHI660 electrochemical working station in a frequency range of 100 kHz to 10 mHz with a 5-mV perturbation at 25 °C.

2.3. Characterizations

The ^{17}O nuclear magnetic resonance (NMR) spectra of the electrolytes were performed on a 500 MHz Varian NMR Inova spectrometer with a Nalorac 5 mm dual-broadband probe tuned to 67.76 MHz at 30 °C with pure electrolyte solutions [34]. The 1d pulse sequence used incorporated a 15 μs 90° radiofrequency pulse, 50 ms acquisition time, and 0.2 s recycle delay [34]. Raman spectra were recorded using an inverted optical microscope (Nikon Ti-E) coupled to a Raman spectrometer (LabRam HR, Horiba). Spectra were recorded using minimal power (50 μW) from a 633 nm laser source, which was delivered to the samples using a 10X air objective [35]. The viscosity (η) of the electrolytes was measured on a Brookfield DV-II+ Pro-Viscometer at 30 °C. The ionic conductivity of the electrolytes was tested on a fully integrated multi-channel conductivity spectrometer (BioLogic MCS10) with conductivity cells made of two parallel Pt electrodes. The cell constant number was calibrated with 0.1 M KCl solution.

For postmortem analyses using scanning electron microscopy (SEM), X-ray photoelectron spectroscopy (XPS), and transmission electron microscopy (TEM) measurements, cycled coin cells were disassembled inside the glovebox to collect the desired electrodes. These electrodes were rinsed with fresh anhydrous DME solvent (300 μL) to remove residual electrolytes, dried under vacuum and then sealed in airtight containers in the glovebox. SEM images were performed on a Helios focused ion

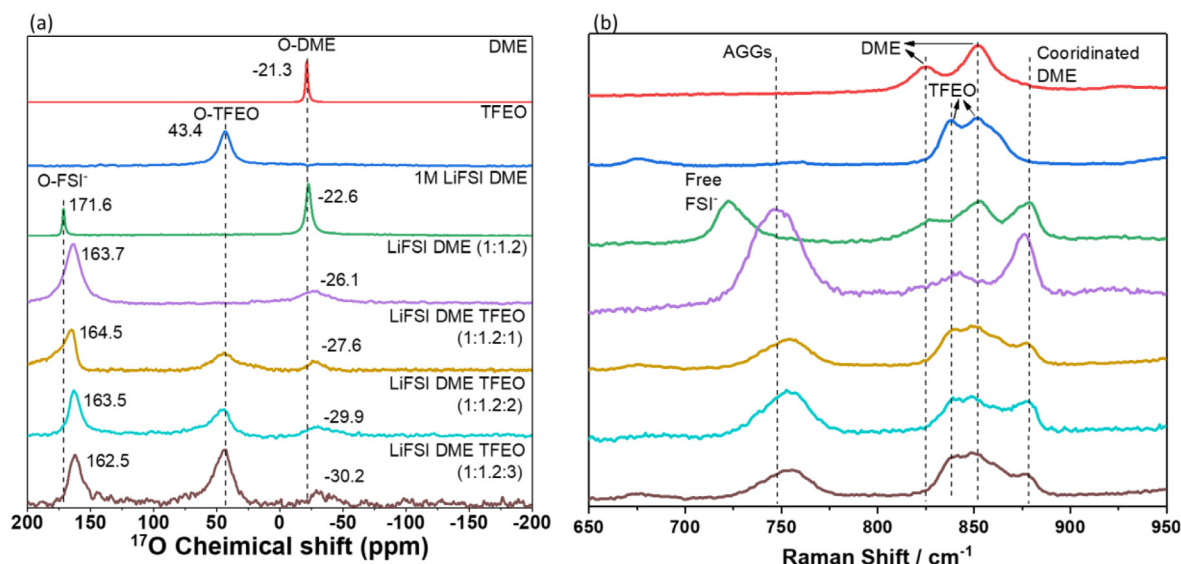


Fig. 1. (a) ^{17}O -NMR spectra and (b) Raman spectra of different solvents and electrolytes with different LiFSI concentrations and TFEO ratios.

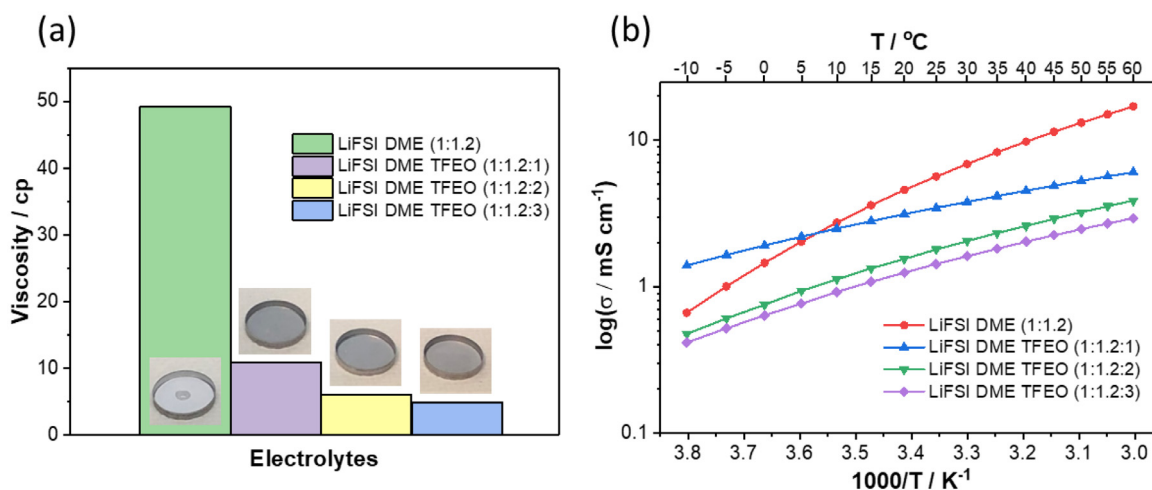


Fig. 2. Physical properties of the studied electrolytes. (a) Viscosity and wettability on PE separator at 30 °C, and (b) ionic conductivity at different temperatures.

beam (FIB)-SEM at an accelerating voltage of 5 kV and a current of 86 pA [24]. XPS measurements were carried out on a Physical Electronics Quanterra scanning X-ray microprobe with a focused monochromatic Al $K\alpha$ X-ray (1486.7 eV) source for excitation and a spherical section analyzer and a pass energy of 69.0 eV for high-energy-resolution spectra collection [24]. The depth profiling investigation was tested with sputtering parameters of Ar⁺ ions, 2 kV, 2 μA , 45° incident angle [24]. The sputtering depth increments for the Li metal samples were 0, 3, 6, 10 nm referred to SiO₂ [24]. The sputtering depth increments for the NMC811 samples were 0, 5, 10, 15, 20 nm referred to SiO₂ [24]. FEI Helios Dual Beam system was used to prepare the TEM samples. A randomly selected secondary NMC811 particle underwent a lift-out process. The targeted particle was coated with a $\sim 2 \mu\text{m}$ Pt layer and was then extracted along with the capping layers and welded to the TEM grid, [38] followed by a thinning processes at 30 kV, 5 kV and then 2 kV to polish the surface and remove the damaged layers [38]. The as-prepared TEM sample was imaged on a JEOL JEM-ARM200CF spherical-aberration-corrected microscope, with the convergence angle of 20.6 mrad for imaging, and the signals of 90–370 mrad for high-angle annular dark-field scanning transmission electron microscopy (HADF-STEM) and 10–23 mrad for annular bright-field STEM (ABF-STEM) imaging [38].

3. Results and discussion

As mentioned in introduction, although an HCE, such as 4 M LiFSI in DME, exhibits high Li CE and good cycling stability, [39] it also exhibits high viscosity. TFEO, with low polarity and high symmetry, doesn't dissolve conductive salts, such as LiFSI, effectively, and can be considered a diluent [24]. In this work, a series of electrolytes with different DME to TFEO ratios have been investigated by ^{17}O -NMR (Fig. 1a) and Raman spectroscopy (Fig. 1b) to obtain a fundamental understanding of the evolving electrolyte solvation structures with the addition of TFEO. As references, two LiFSI/DME electrolytes without TFEO were also investigated: one is a diluted electrolyte with a LiFSI:DME molar ratio of 1:9, and the other is an HCE with a LiFSI:DME molar ratio of 1:1.2.

By increasing the LiFSI content in DME from 0 (pure DME) to 1:9 (dilute electrolyte) and 1:1.2 (HCE), the ^{17}O signal of DME shifts from -22.6 to -26.1 and -27.6 ppm respectively, which indicates that the coordination between DME and Li⁺ is increased by increasing the LiFSI concentration. Additionally, the ^{17}O signal of sulfonyl oxygen atoms in the FSI⁻ anion also shifts from 171.6 to 163.7 ppm with an increased LiFSI:DME molar ratio from 1:9 to 1:1.2, which is most likely a result of increased ion-dipole interactions between the Li⁺ and FSI⁻ in

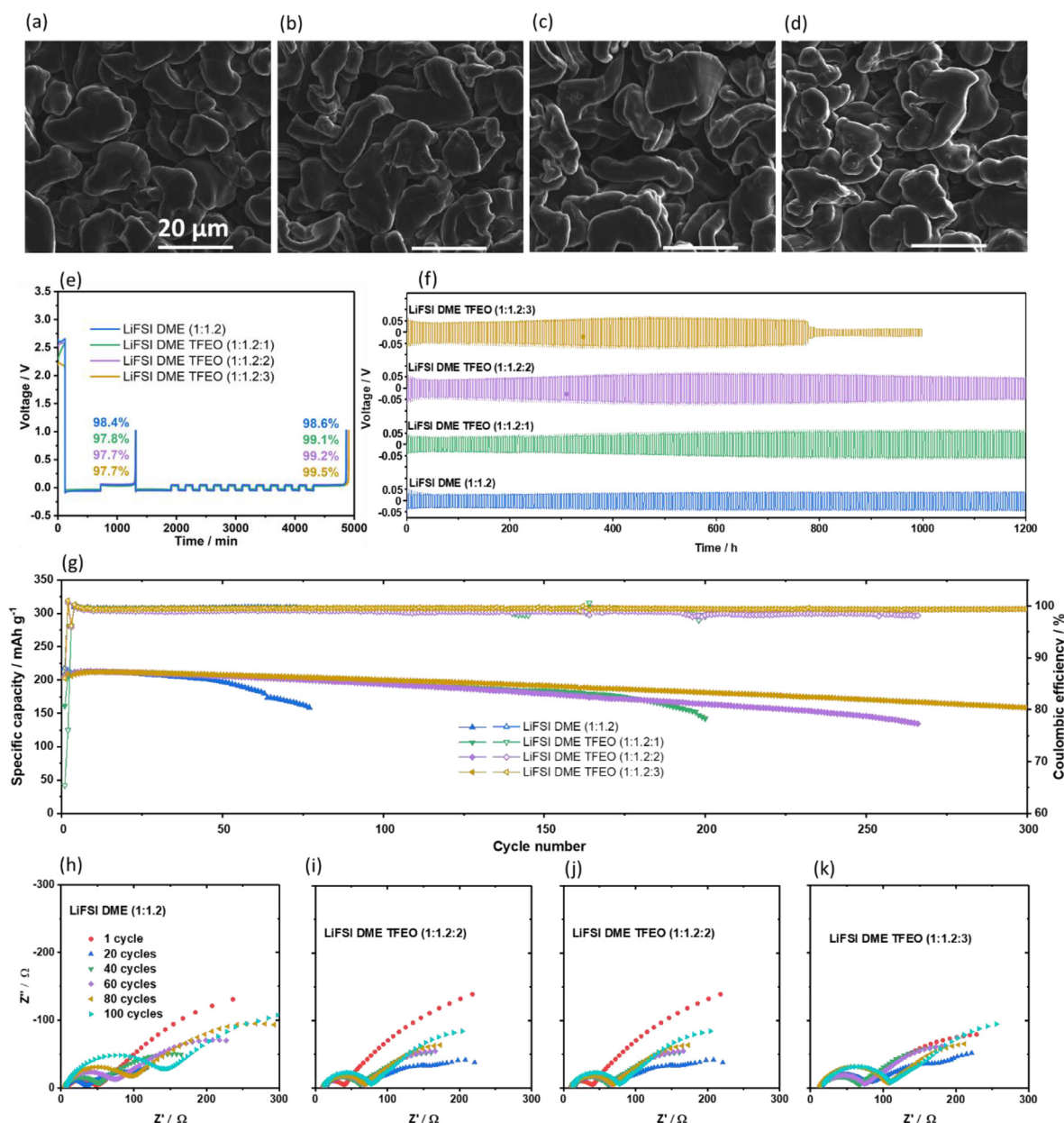


Fig. 3. Li metal deposition morphologies and electrochemical performances in different electrolytes. (a–d) SEM images of deposited Li films (current density of 0.5 mA cm^{-2} and capacity of 1 mAh cm^{-2}) in different electrolytes: (a) LiFSI-1.2DME, (b) LiFSI-1.2DME-TFEO, (c) LiFSI-1.2DME-2TFEO and (d) LiFSI-1.2DME-3TFEO. (e) Li CE in Li||Cu cells, (f) Li||Li symmetric cell cycling (current density of 0.5 mA cm^{-2} and capacity of 1 mAh cm^{-2}) and (g) Li||NMC811 cell performance under moderate testing condition (1.5 mAh cm^{-2} NMC811, 50 μm Li and 75 μL electrolyte). (h–k) Impedance evolution over 100 cycles in the Li||NMC811 cells with different electrolytes, (h) LiFSI-1.2DME, (i) LiFSI-1.2DME-TFEO, (j) LiFSI-1.2DME-2TFEO and (k) LiFSI-1.2DME-3TFEO. The Li||NMC811 cells were cycled at C/3 charge/discharge with a CV charge step at 4.4 V till current reduced to C/20 or 1 hour after two formation cycles at C/10, and 1C capacity is defined as 1.5 mAh cm^{-2} .

the concentrated LiFSI electrolyte [23]. The fact that the sharp signal (171.6 ppm) in the dilute electrolyte becomes broader (163.7 ppm) in the concentrated electrolyte also indicates a more complex coordination structure in the HCE [23]. When TFEO is added into the high concentration LiFSI/DME electrolyte, the shift of oxygen atoms in FSI⁻ (163.5 ppm) and oxygen atoms in TFEO (44.0 ppm) are almost negligible with a shift variation within 1 ppm , while the signal of oxygen atoms in the DME shifts upfield from -26.1 ppm in HCE to -27.6 , -29.9 and -30.2 ppm in LHCEs with TFEO ratios of 1, 2 and 3, respectively. These results indicate that TFEO has minimal interactions with either Li⁺ or FSI⁻, and likely separates large ion clusters in the HCE while not inter-

rupting the strong interactions between Li⁺ and FSI⁻. Instead, the DME further shifts upfield because of the affinity between DME and TFEO diluent.

The recorded Raman spectra support the insights gained from the NMR investigations. As illustrated in Fig. 1b, free DME exhibits vibrational modes at 825 and 853 cm^{-1} , TFEO exhibits vibrational modes at 838 and 853 cm^{-1} , and LiFSI shows vibrational modes at 760 and 777 cm^{-1} [35]. When LiFSI is added into DME, forming the LiFSI-9DME dilute electrolyte, a peak at 722 cm^{-1} is formed, which can be assigned to the uncoordinated FSI⁻.³⁵ The peak at 878 cm^{-1} is related to Li⁺ coordinated DME. Note that the free DME still persists in the

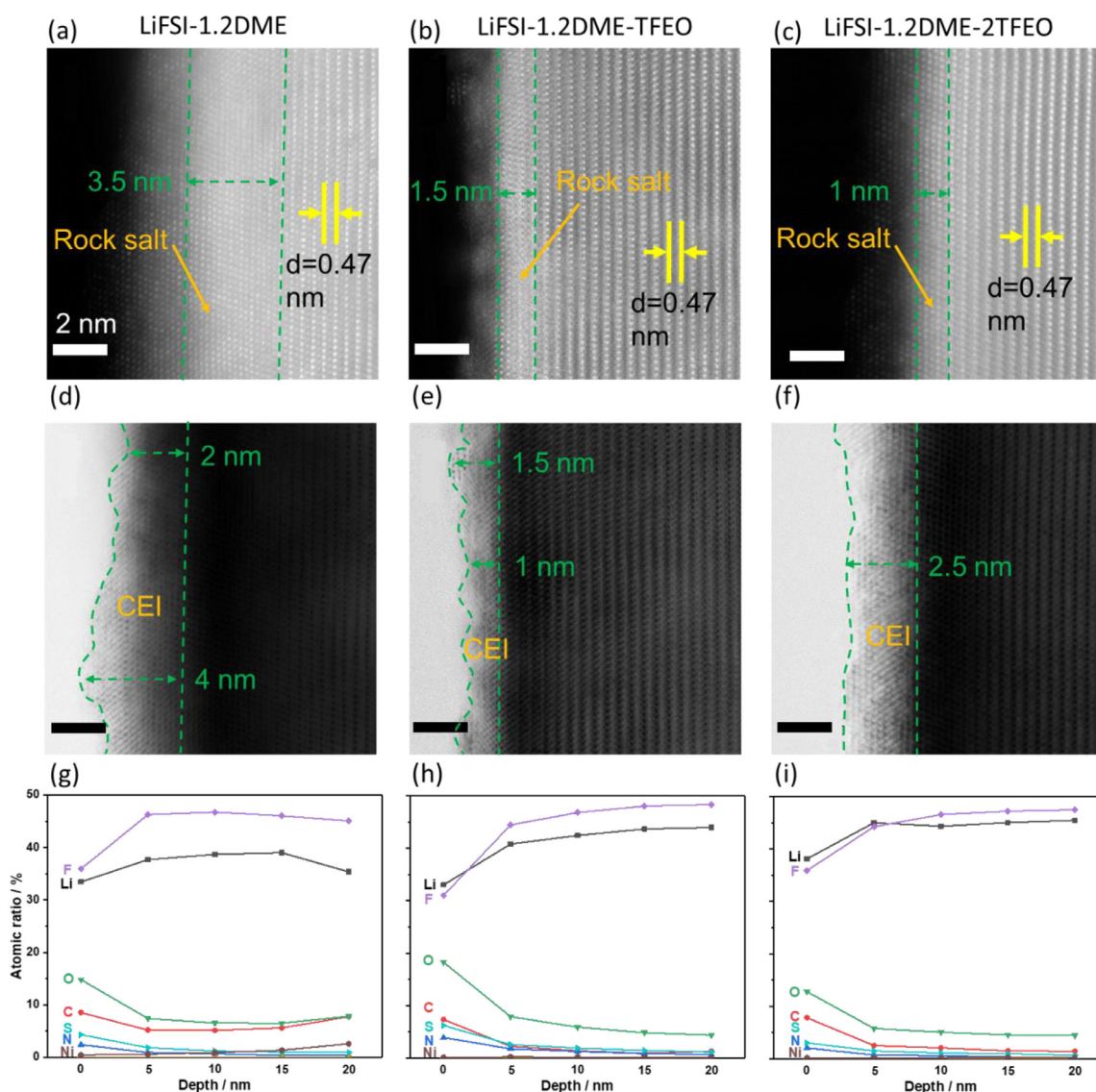


Fig. 4. Structural images and CEI compositions of the cycled NMC 811 electrodes. (a-c) HAADF-STEM, (d-f) ABF-STEM images and (g-i) atomic ratios of elemental evolution with depth profiling in CEIs from XPS results (referred to SiO_2) of cycled NMC811 after 100 cycles. (a, d, g) LiFSI-1.2DME, (b, e, h) LiFSI-1.2DME-TFEO and (c, f, i) LiFSI-1.2DME-2TFEO. The Li||NMC811 cells were cycled at C/3 charge/discharge with a CV charge step at 4.4 V till current decreased to C/20 or 1 h after two formation cycles at C/10, and 1C is 1.5 mA cm^{-2} .

sample, and is marked by its characteristic 825 cm^{-1} vibrational resonance. When the LiFSI concentration increases to LiFSI-1.2DME HCE, the peaks associated with free DME (at 825 cm^{-1}) and uncoordinated FSI^- disappear. A new peak at 748 cm^{-1} is observed, which can be assigned to the CIPs and AGGs in which FSI^- is coordinated to two or more Li^+ ions. With further addition of TFEO, no free DME signatures were observed in all three LiFSI-1.2DME-xTFEO (where $x = 1, 2$ and 3) electrolytes while AGGs are still well-preserved, confirming that TFEO does not perturb the solvation structures of Li^+ and FSI^- . In addition, the resonance that arises from AGGs shifts slightly to higher frequencies, indicating an even stronger coordination of AGGs exists in the LiFSI-1.2DME-xTFEO electrolytes. Based on these results, we can conclude that TFEO is an excellent diluent that may be used in LHCEs.

The effects of TFEO on the physical properties of electrolytes (including their wettability to the separator, viscosity, and ionic conductivity) were further investigated at different temperatures. As shown in Fig. 2a, the HCE of LiFSI-1.2DME has a high viscosity of 49.2 cP at 30°C , which

makes it difficult to wet the PE separator and electrodes. In contrast, with the addition of TFEO, the viscosities of the TFEO based electrolytes significantly decrease to 10.9, 6.03 and 4.86 cP at TFEO molar ratios of 1, 2 and 3, respectively. These low viscosity electrolytes have great wettability with the PE separator, as shown in Fig. 2a.

However, the ionic conductivity of these electrolytes is decoupled from their viscosity (fluidity). Considering the associated Li^+ and FSI^- states in CIPs and AGGs, Li^+ is expected to move in a hopping manner, in both the HCE and the TFEO based LHCEs, similar to the hopping-type ion-transport in inorganic solid ionic conductors. Therefore, with increasing amounts of TFEO, the overall LiFSI concentration decreases in the electrolytes and leads to a relatively lower ionic conductivity in the LHCEs. The salt concentrations in these four electrolytes are 4.8, 2.4, 1.6 and 1.0 M when TFEO molar ratios in these electrolytes increases from 0 to 1, 2 and 3, respectively. Nevertheless, the ionic conductivities of the HCE and LHCEs are $5.65, 3.46, 1.79$ and 1.43 mS cm^{-1} at 25°C , respectively, which are still sufficient for ion transport in batteries, where the kinetic bottleneck still lies on the interphases.

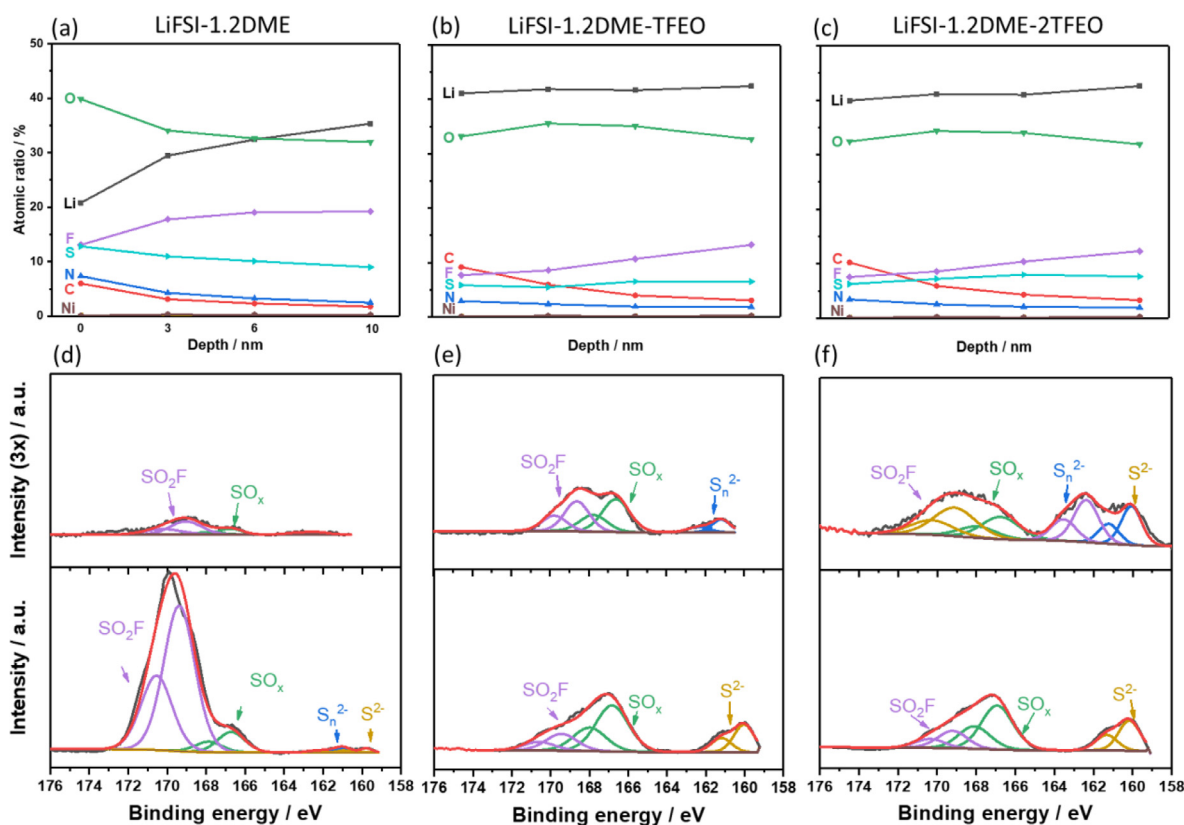


Fig. 5. XPS results of SEIs on cycled Li anodes in different electrolytes. (a-c) XPS depth profiling of Li anodes after 100 cycles in Li||NMC811 cells. (d-f) S 2p spectra of Li anodes after 2 formation cycles (top) and 100 cycles (bottom) in three different electrolytes. (a, d) LiFSI-1.2DME, (b, e) LiFSI-1.2DME-TFEO and (c, f) LiFSI-1.2DME-2TFEO. The Li||NMC811 cells were cycled at C/3 charge/discharge with a CV charge step at 4.4 V till current to C/20 or 1 h after two formation cycles at C/10, and 1C is defined as 1.5 mA cm⁻².

3.1. Electrolyte performance under moderate testing condition

As shown in Figs. 3a-3d, the deposited Li, in the four electrolytes (HCE and LHCEs) investigated in this work, are large granular shaped particles (not in dendritic form) with most particles greater than 10 μm. These large Li particles exhibit smaller surface-to-volume ratios, which are beneficial for high Li CE, as shown in Fig. 3e. The initial CE is 98.4% for HCE and 97.8%, 97.7% and 97.7% respectively for three LHCEs with TFEO molar ratios between 1 and 3. As for the average CE, the LHCEs show slightly higher CEs of 99.1%, 99.2% and 99.5% than that of HCE (98.6%). Fig. 3f shows the cycling performance of Li||Li symmetric cells with these four electrolytes at a current density of 0.5 mA cm⁻² and an areal capacity of 1 mAh cm⁻². As the TFEO amount increases, the overpotential of Li plating/stripping during initial cycles increases slightly, which can be attributed to the decreased ionic conductivity as the TFEO amounts in the electrolyte increases (Fig. 2b). In addition, a long cycling time of over 1200 h was obtained for the Li||Li cells with a HCE and two LHCEs containing TFEO at 1 and 2 molar ratios, but when the TFEO molar ratio was further increased to 3, the Li||Li cells only lasted for approximately 800 h before short circuiting occurred. These results are much better than that of the state-of-the-art carbonate electrolyte (1 M LiPF₆/ ethylene carbonate (EC)-ethyl methyl carbonate (EMC) + 2 wt.% vinylene carbonate (VC)) under the same conditions, which was stable for only around 300 h [24].

When paired with a high voltage cathode NMC811, the 1 and 2 molar ratio TFEO based LHCEs showed much longer cycling stability than the HCE, and the cycle number increased as the molar ratio of TFEO increased (Fig. 3g). The LHCE of LiFSI-1.2DME-3TFEO lead to more than 300 stable cycles of Li||NMC811 cells under the moderate testing condition with 1.5 mAh cm⁻² NMC811 cathode, 50 μm Li and 75 μl electrolyte

in the CR2032 coin cells. Figs. 3h-3k show the impedance evolution of the Li||NMC811 cells with the investigated electrolytes during the first 100 cycles at 20 cycle intervals. For the cell with the HCE (Fig. 3h), the impedance continually increased during cycling and the combination of SEI resistance (R_{SEI}) and charge transfer resistance (R_{ct}) increased from around 30 to 150 Ω after 100 cycles. The impedances of the cells with three LHCEs were much more stable during cycling. From an impedance point of the view, the most stable LHCE is LiFSI-1.2DME-2TFEO, where the total value of R_{SEI} and R_{ct} is around 80 Ω after 100 cycles, which is about half of that found in the cell with HCE.

The improved performance of the Li||NMC811 cell as the amount of TFEO increased in the electrolyte, during moderate testing conditions, can be explained mainly by the CEI properties and the structural stability of the NMC811 electrodes. Figs. 4a-4f show the HAADF-STEM and ABF-STEM images of the NMC811 electrodes after they were cycled in different electrolytes for 100 cycles. As reported in the previous works, the pristine NMC811 electrode has a clear layered structure (Figure S1a) [23,24]. For the electrode cycled in HCE, the surface undergoes a phase transition due to the electrolyte and NMC811 interactions. A disordered rock salt phase approximately 3.5 nm thick was found on the surface of the layered cathode, outlined by the green dashed lines in Fig. 4a. This reconstruction of the lattice structure also occurred in the NMC811 electrodes cycled in two LHCEs of LiFSI-1.2DME-TFEO and LiFSI-1.2DME-2TFEO but with a much thinner rock salt thicknesses of ~1.5 nm (Fig. 4b) and ~1 nm (Fig. 4c), respectively. When the TFEO molar ratio was further increased to 3 (i.e. LiFSI-1.2DME-3TFEO), the electrode surface maintained a layered structure (Figure S1d) that is comparable to the pristine sample (Figure S1b) as reported before [24].

The cause of the suppressed lattice reconstruction in the three LHCEs can be attributed to the formation of more protective LiF-rich CEI lay-

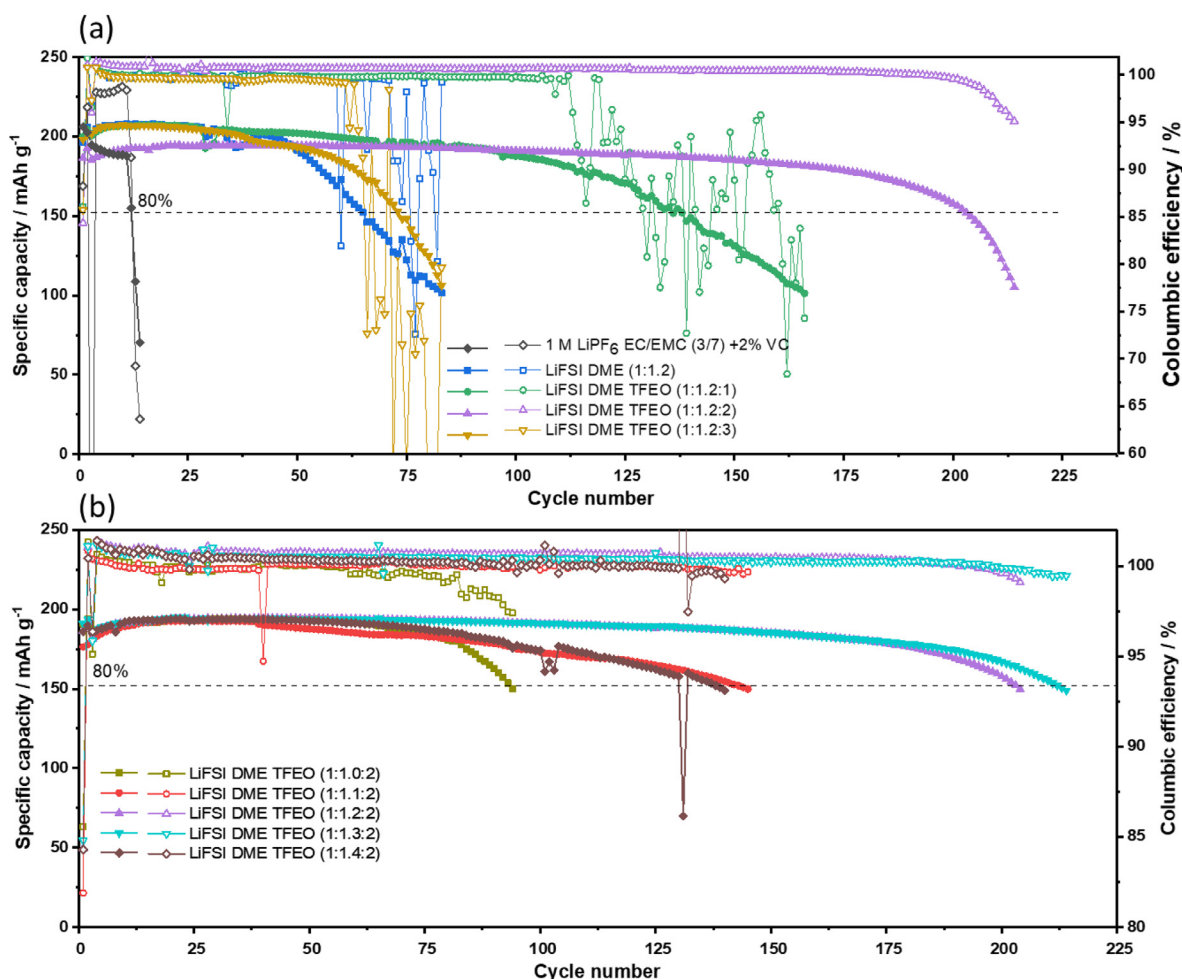


Fig. 6. Cycling performance of Li||NMC811 cells under practical conditions. (a) Li||NMC811 cells in different electrolytes with different amounts of TFEO, (b) Li||NMC811 cells in different electrolytes with different amounts of DME. Cells are using 50 μm Li anode, 4.2 mAh cm^{-2} NMC811 cathode, and lean electrolyte of 15 μL per coin cell. Cells were charged at C/10 and discharged at C/3 after two formation cycles at C/10 charge and discharge, where 1C is defined as 4.2 mA cm^{-2} .

ers in these electrolytes as shown in the corresponding ABF-STEM images (Figs. 4d–4f and S1c). In the HCE, a CEI layer with a thickness ranging from 2 to 4 nm is found on the NMC811 surface and is partially crystalline. Figs. 4g–4i show a summary of the atomic ratio of elemental distribution in each CEI at different depths using XPS measurements. These XPS data indicate that LiF is the dominate phase in the CEI. When the TFEO is introduced to the HCE, the LiFSI-1.2DME-TFEO leads to a much thinner CEI (1.5 nm) with higher LiF crystallinity and suppressed lattice reconstruction; therefore, although this CEI is thin, it is effective at suppressing the side reactions between the NMC811 surface and the electrolyte, and limiting the lattice reconstruction caused by the Li/Ni cation mixing. When the molar ratio of TFEO is further increased, the CEI thickness increases (2.5 nm in LiFSI-1.2DME-2TFEO (see Fig. 4f) and 5 nm in LiFSI-1.2DME-3TFEO (see Fig. S1c) with an even higher LiF crystallinity (Fig. S2a). With the excellent protection of a 5 nm CEI (dominated by LiF) in LiFSI-1.2DME-3TFEO, the detrimental phase transition was effectively suppressed and almost eliminated in this electrolyte [24].

In addition to the stability of the NMC811 cathode, the stability of the LMA and electrolyte also plays a critical role in the performance of Li||NMC811 cells. An electrolyte which is highly stable with LMA is essential for long-term cycling stability of LMBs. It is generally accepted that the performance of LMAs is mainly determined by the quality of the SEI layer, and that a homogeneous and compact SEI layer is essential to effectively suppress the continuous electrolyte/Li interaction and to sta-

bilize the LMA. Figs. 5a–5c and S2b show the atomic ratios of elemental distribution in the SEI layer of the cycled Li anode at different depths. The HCE results in more O atoms on the surface than Li and F atoms (Fig. 5a). For the TFEO containing electrolytes, very similar elemental distributions are found in all three LHCEs as shown in Figs. 5b, 5c and S2b. Li exhibits the highest atomic ratio in the SEI layer formed on the LMA after 100 cycles in Li||NMC811 cells, while O exhibits the second highest atomic ratio.

Two of the most apparent differences in the SEIs formed in HCE and TFEO based LHCEs are: (1) the SEI formed in LHCEs have a much smaller F content, and much higher Li and O contents than those formed in HCE, indicating that Li₂O_x is the dominant component in SEIs formed in LHCEs under the given testing condition; and (2) SEIs formed in LHCEs exhibit significantly improved homogeneity through their thicknesses as compared to the large variation of atomic ratios observed along the thickness of the SEI layer formed in HCE. This highly homogenous, Li₂O_x-rich SEI is very efficient in protecting the LMA during cycling under the given testing condition.

The S 2p spectra shown in Figs. 5d–df and S3 provide solid evidence to support this conclusion based on the LiFSI decomposition during SEI formation and evolution. The top figures are the spectra after 2 formation cycles while the bottom ones are after 100 cycles. In the HCE (Fig. 5d), only a small amount of LiFSI decomposes in the formation cycles but the LiFSI continuously decomposes during the 100 cycles. In contrast, when TFEO is added to the LHCEs, the LiFSI decomposition

is accelerated in the formation cycles and thus the SEIs are very stable against further decomposition of the electrolyte. An interesting observation in S 2p spectra is that the LiFSI is more completely reduced (as suggested by the higher intensity of S^{2-} signal (originally S is at 6+ valent in LiFSI)), after the formation cycles, in the electrolyte with higher ratios of TFEO. The reason for this could be attributed to the lower overall LiFSI concentration in the electrolyte with higher TFEO ratios, where less of the LiFSI is available to interact with the Li metal to form the SEI in the initial state. This difference disappears after 100 cycles and then the SEI compositions in three LHCEs are very similar. This may occur because the supplemental LiFSI in the electrolyte, under a flooded electrolyte condition, minimizes the influence of varying salt concentrations in the electrolytes. However, when it comes to the lean electrolyte condition, it could be different because of the very limited LiFSI amount available in the cells. This situation will be further discussed later.

3.2. Cycling performance of Li||NMC811 cells under practical testing condition

To evaluate the performances of the LHCEs under practical LMB applications, Li||NMC811 cells with these electrolytes were tested under highly challenging conditions, combining a high-loading (4.2 mAh cm^{-2}) cathode, a thin Li anode (thickness of $50 \mu\text{m}$, N/P at ~ 2), and a practical amount of electrolyte (E/C ratio of 3 g (Ah)^{-1} (i.e. $15 \mu\text{L}$) in each coin cell), which are consistent with the parameters applied in the pouch cells for high energy density LMBs [4,23]. As shown in Fig. 6a, the cell using the conventional carbonate electrolyte could last only 10 cycles before a sudden failure occurred. The failure was due to severe side reactions between the electrolyte and the Li anode, which lead to the depletion of the electrolyte or Li, or created high cell impedance. When using an HCE, the cell showed improved cycling stability because of better Li stability in the HCE. With the addition of TFEO, the cycling performance of the cells increases when the TFEO ratio increased from 1 to 2 (i.e. from LiFSI-1.2DME-TFEO to LiFSI-1.2DME-2TFEO). Cycle life of the cell with 80% capacity retention was increased from 125 cycles in LiFSI-1.2DME-TFEO to 205 cycles in LiFSI-1.2DME-2TFEO under these challenging conditions. However, when the TFEO molar ratio further increased to 3 in LiFSI-1.2DME-3TFEO, the cycle life of the cell with this electrolyte was much shorter than with the other two TFEO electrolytes. This result is very different from what was observed in the moderate condition as shown in Fig. 3g, where the electrolyte with a TFEO molar ratio of 3 showed the longest cycling stability.

This inconsistent behavior can be explained by the difference in the absolute salt amount in the electrolytes. Under the moderate test conditions, $75 \mu\text{L}$ electrolyte was used for a 1.5 mAh cm^{-2} NMC811 cathode ($1.88 \text{ mAh per electrode (} 1.25 \text{ cm}^2)$). In contrast, under the practical conditions, $15 \mu\text{L}$ electrolyte was used for a 4.2 mAh cm^{-2} NMC811 cathode ($5.25 \text{ mAh per electrode}$). This means 14 times more electrolyte per mAh was used under moderate conditions compared to the practical conditions. As shown in Fig. 5, the SEIs formed in the HCE and LHCEs are mainly derived from the salt decomposition, thus the absolute amount of decomposed LiFSI could lead to an apparent LiFSI concentration decrease under the lean electrolyte condition when the original amount of salt is limited in a highly diluted electrolyte such as LiFSI-1.2DME-3TFEO. On the other hand, when the amount of electrolyte increases 14 times, as it did in the moderate condition tests, salt loss during the SEI formation process has a negligible effect on the total salt concentration of the electrolyte. This LiFSI decomposition is also not a problem in the HCE and the LHCEs of LiFSI-1.2DME-TFEO and LiFSI-1.2DME-2TFEO because much higher overall salt concentrations exist in these electrolytes, which are 4.8 M for HCE, 2.4 M and 1.6 M for LiFSI-1.2DME-TFEO and LiFSI-1.2DME-2TFEO respectively, while 1 M is for LiFSI-1.2DME-3TFEO. Consequently, the LiFSI-1.2DME-2TFEO shows the longest cycling performance in Li||NMC811 cells under the practical condition.

Moreover, efforts were also made to tune the DME amount in the electrolytes of LiFSI-yDME-2TFEO (where $y = 1.0$ to 1.4) to gain the best cycling performance under practical conditions. As shown in Fig. 6b, the optimized DME ratio was found to be 1.3, i.e. LiFSI-1.3DME-2TFEO. The cell with this electrolyte retains 80% capacity in 215 cycles under practical conditions. These results demonstrate that TFEO based LHCEs are highly promising for further improvement of high energy density LMBs.

4. Conclusions

We have demonstrated that TFEO acts as an effective diluent in HCEs to form LHCEs, which not only exhibit low viscosity and good wettability, but also lead to the formation of highly robust and protective interphases on both the Ni-rich NMC811 cathode (CEI) and the LMA (SEI) that suppress detrimental side reactions. TFEO based LHCEs can minimize lattice reconstruction from layered structure to rock salt structure on NMC811 cathode and suppress the continuous SEI growth on LMAs. As a result, the cycling performance of Li||NMC811 cells can be significantly improved. Under highly demanding conditions required by practical applications, i.e. high-loading cathode, thin Li anode and lean electrolyte, the LHCEs of LiFSI-1.2DME-2TFEO and LiFSI-1.3DME-2TFEO have enabled high energy density LMBs to retain more than 80% capacity over 200 cycles. Furthermore, this work reveals that the main factors determining the cell cycling performance depend on the cell testing conditions: Great CEI properties and cathode stability are crucial under moderate cathode loading and flooded electrolyte conditions, while balanced CEI properties and sufficient salt concentration, for salt-derived SEI formation, determine the cell performance under the practical condition where only a minimum amount of electrolyte is available. These crucial findings highlight the importance of electrode/electrolyte interphase chemistries and the criteria for designing an electrolyte under practical conditions. The optimized electrolytes can be combined other battery design parameters, including stable electrodes and separator to enable the safe operation of practical high energy density LMBs.

Author contributions

J.-G.Z., W.X. and X.C. proposed the research and designed the experiments. X.C. performed the electrochemical measurements and conducted the SEM observations with help from L.C.Z., X.H., X.R. and H.-S.L. L.F.Z., B.E.M., B.W.A. and C.W. performed the FIB and TEM. M.H.E. performed XPS measurements. S.D.B performed ^{17}O NMC measurements. P.Z.E. carried out the Raman measurements. C.N. and H.L. prepared the NMC811 electrodes. X.C., W.X. and J.-G.Z. prepared the manuscript with input from all other coauthors.

Data availability

The data that support the plots within these paper and other findings of this study are available from the corresponding authors upon request.

Declaration of Competing Interest

The authors declare no competing interests.

Acknowledgements

This work is supported by the Assistant Secretary for Energy Efficiency and Renewable Energy, Vehicle Technologies Office, of the U.S. Department of Energy (DOE) through the Advanced Battery Materials Research (BMR) program (Battery500 Consortium) under contract no. DE-AC05-76RL01830. The SEM, TEM, Raman and XPS measurements were performed using EMSL (grid.436923.9), a DOE Office of Science User Facility sponsored by the Office of Biological and Environmental Research located at Pacific Northwest National Laboratory (PNNL).

PNNL is operated by Battelle for the DOE under Contract DE-AC05-76RL01830. The LiFSI salt was provided by Dr. Kazuhiko Murata of Nippon Shokubai Co., Ltd.

References

- [1] M. Armand, J.M. Tarascon, Building better batteries, *Nature* 451 (2008) 652, doi:10.1038/451652a.
- [2] Y. Zhang, et al., Towards better Li metal anodes: Challenges and strategies, *Mater. Today* 33 (2019) 56–74, doi:10.1016/j.mattod.2019.09.018.
- [3] F. Wu, et al., Perspectives for restraining harsh lithium dendrite growth: Towards robust lithium metal anodes, *Energy Storage Mater.* 15 (2018) 148–170.
- [4] C. Niu, et al., High-energy lithium metal pouch cells with limited anode swelling and long stable cycles, *Nature Energy* 4 (2019) 551–559, doi:10.1038/s41560-019-0390-6.
- [5] M.S. Whittingham, Ultimate Limits to Intercalation Reactions for Lithium Batteries, *Chem. Rev.* 114 (2014) 11414–11443, doi:10.1021/cr5003003.
- [6] R. Bouchet, Batteries: A stable lithium metal interface, *Nat. Nanotechnol.* 9 (2014) 572–573, doi:10.1038/nnano.2014.165.
- [7] J.-G. Zhang, W. Xu, W.A. Henderson, in: *Lithium Metal Anodes and Rechargeable Lithium Metal Batteries*, XV, Springer International Publishing, 2017, p. 194.
- [8] G. Crabtree, The coming electric vehicle transformation, *Science* 366 (2019) 422–424, doi:10.1126/science.aax0704.
- [9] A. Zhamu, et al., Reviving rechargeable lithium metal batteries: enabling next-generation high-energy and high-power cells, *Energy Environ. Sci.* 5 (2012) 5701–5707, doi:10.1039/C2EE02911A.
- [10] J. Liu, et al., Pathways for practical high-energy long-cycling lithium metal batteries, *Nature Energy* 4 (2019) 180–186, doi:10.1038/s41560-019-0338-x.
- [11] F. Lin, et al., Surface reconstruction and chemical evolution of stoichiometric layered cathode materials for lithium-ion batteries, *Nat. Commun.* 5 (2014) 3529, doi:10.1038/ncomms4529.
- [12] Y.-K. Sun, et al., High-energy cathode material for long-life and safe lithium batteries, *Nat. Mater.* 8 (2009) 320–324 http://www.nature.com/nmat/journal/v8/n4/supinfo/nmat2418_S1.html.
- [13] X. Yu, A. Manthiram, Electrode–electrolyte interfaces in lithium-based batteries, *Energy Environ. Sci.* 11 (2018) 527–543, doi:10.1039/C7EE02555F.
- [14] J. Xiao, How lithium dendrites form in liquid batteries, *Science* 366 (2019) 426–427, doi:10.1126/science.aay8672.
- [15] W. Xu, et al., Lithium metal anodes for rechargeable batteries, *Energy Environ. Sci.* 7 (2014) 513–537, doi:10.1039/C3EE40795K.
- [16] W. Zhao, et al., High Voltage Operation of Ni-Rich NMC Cathodes Enabled by Stable Electrode/Electrolyte Interphases, *Adv. Energy Mater.* 8 (2018) 1800297, doi:10.1002/aenm.201800297.
- [17] R. Petibon, et al., Electrolyte System for High Voltage Li-Ion Cells, *J. Electrochem. Soc.* 163 (2016) A2571–A2578, doi:10.1149/2.0321613jes.
- [18] X. Qi, et al., Lifetime limit of tris(trimethylsilyl) phosphite as electrolyte additive for high voltage lithium ion batteries, *RSC Adv.* 6 (2016) 38342–38349, doi:10.1039/C6RA06655D.
- [19] K. Xu, Nonaqueous Liquid Electrolytes for Lithium-Based Rechargeable Batteries, *Chem. Rev.* 104 (2004) 4303–4418, doi:10.1021/cr030203g.
- [20] L. Cheng, et al., Accelerating Electrolyte Discovery for Energy Storage with High-Throughput Screening, *J. Phys. Chem. Lett.* 6 (2015) 283–291, doi:10.1021/jz502319n.
- [21] J. Schaefer, et al., Electrolytes for high-energy lithium batteries, *Appl. Nanosci.* 2 (2012) 91–109, doi:10.1007/s13204-011-0044-x.
- [22] S. Chen, et al., High-Efficiency Lithium Metal Batteries with Fire-Retardant Electrolytes, *Joule* 2 (2018) 1548–1558, doi:10.1016/j.joule.2018.05.002.
- [23] X. Ren, et al., Enabling High-Voltage Lithium-Metal Batteries under Practical Conditions, *Joule* 3 (2019) 1662–1676 <https://doi.org/>, doi:10.1016/j.joule.2019.05.006.
- [24] X. Cao, et al., Monolithic solid–electrolyte interphases formed in fluorinated orthoformate-based electrolytes minimize Li depletion and pulverization, *Nature Energy* 4 (2019) 796–805, doi:10.1038/s41560-019-0464-5.
- [25] X.-B. Cheng, R. Zhang, C.-Z. Zhao, Q. Zhang, Toward Safe Lithium Metal Anode in Rechargeable Batteries: A Review, *Chem. Rev.* 117 (2017) 10403–10473, doi:10.1021/acs.chemrev.7b00115.
- [26] K. Xu, Electrolytes and Interphases in Li-Ion Batteries and Beyond, *Chem. Rev.* 114 (2014) 11503–11618, doi:10.1021/cr500003w.
- [27] S. Chen, et al., High-Voltage Lithium-Metal Batteries Enabled by Localized High-Concentration Electrolytes, *Adv. Mater.* 30 (2018) 1706102, doi:10.1002/adma.201706102.
- [28] J. Chen, et al., Electrolyte design for LiF-rich solid–electrolyte interfaces to enable high-performance micro-sized alloy anodes for batteries, *Nature Energy* (2020), doi:10.1038/s41560-020-0601-1.
- [29] H. Jia, et al., Hierarchical porous silicon structures with extraordinary mechanical strength as high-performance lithium-ion battery anodes, *Nat. Commun.* 11 (2020) 1474, doi:10.1038/s41467-020-15217-9.
- [30] Y. Yamada, J. Wang, S. Ko, E. Watanabe, A. Yamada, Advances and issues in developing salt-concentrated battery electrolytes, *Nature Energy* 4 (2019) 269–280, doi:10.1038/s41560-019-0336-z.
- [31] L. Suo, et al., Water-in-salt” electrolyte enables high-voltage aqueous lithium-ion chemistries, *Science* 350 (2015) 938–943, doi:10.1126/science.aab1595.
- [32] X. Ren, et al., High-Concentration Ether Electrolytes for Stable High-Voltage Lithium Metal Batteries, *ACS Energy Lett.* 4 (2019) 896–902, doi:10.1021/acsenerylett.9b00381.
- [33] L. Yu, et al., A Localized High-Concentration Electrolyte with Optimized Solvents and Lithium Difluoro(oxalate)borate Additive for Stable Lithium Metal Batteries, *ACS Energy Lett.* 3 (2018) 2059–2067, doi:10.1021/acsenerylett.8b00935.
- [34] X. Ren, et al., Localized High-Concentration Sulfone Electrolytes for High-Efficiency Lithium-Metal Batteries, *Chem* 4 (2018) 1877–1892 <https://doi.org/>, doi:10.1016/j.chempr.2018.05.002.
- [35] J. Zheng, et al., Extremely Stable Sodium Metal Batteries Enabled by Localized High-Concentration Electrolytes, *ACS Energy Lett.* 3 (2018) 315–321, doi:10.1021/acsenerylett.7b01213.
- [36] X. Cao, et al., Monolithic solid–electrolyte interphases formed in fluorinated orthoformate-based electrolytes minimize Li depletion and pulverization, *Nature Energy* 4 (2019) 796–805, doi:10.1038/s41560-019-0464-5.
- [37] B.D. Adams, J. Zheng, X. Ren, W. Xu, J.-G. Zhang, Accurate Determination of Coulombic Efficiency for Lithium Metal Anodes and Lithium Metal Batteries, *Adv. Energy Mater.* 8 (2018) 1702097, doi:10.1002/aenm.201702097.
- [38] L. Zou, et al., Solid–Liquid Interfacial Reaction Triggered Propagation of Phase Transition from Surface into Bulk Lattice of Ni-Rich Layered Cathode, *Chem. Mater.* 30 (2018) 7016–7026, doi:10.1021/acs.chemmater.8b01958.
- [39] J. Qian, et al., High rate and stable cycling of lithium metal anode, *Nat. Commun.* 6 (2015) 6362, doi:10.1038/ncomms7362.